PAPER

Check for updates

Constructing helical nanowires *via* polymerization-induced self-assembly†

Qiumeng Chen,[a] Yahui Li,[a] Ming Liu,[a] Xuan Wu,[b] Jianliang Shen [ID] *[ab] and Liangliang Shen [ID] *[a]

While reliable strategies for constructing block copolymer (BCP) nanowires have been developed, helical nanowires are rarely reported in polymerization-induced self-assembly (PISA). Herein, in this work, a new strategy for constructing helical nanowires was developed *via* PISA mediated by a fluorinated stabilizer block. Ultralong nanowires with helical structure can be readily produced in a wide range of block compositions. In addition, the generality of this strategy was well testified by expanding monomer types. The achiral BCP nano-objects underwent a morphology transition from spheres to helical nanowires during aging. We believe this work will provide a general strategy for producing helical nanowires through PISA of achiral BCPs.

Introduction

Helix is a fascinating structural feature in nature due to its asymmetry, extraordinary aspect ratio, elasticity, aesthetic and chirality.[1–3] In particular, helix is commonly adopted in bio-macromolecules and life, such as DNA,[4] collagen[5] and tobacco mosaic virus.[6] Inspired by nature, construction of helical nanostructures *via* self-assembly of synthetic block copolymers (BCPs) has attracted considerable attention.[7,8] For example, Ho and co-worker elucidated the chirality transfer from molecular level to self-assembled helical phase of polylactide-containing BCP *via* the twisting and shifting.[9] Xu *et al.* reported the successful preparation of helical toroids *via* self-assembly of polypeptide homopolymer and its BCP.[10]

Over the past decade, polymerization-induced self-assembly (PISA) has been extensively investigated as a powerful strategy for the synthesis of BCP nanostructures with controllable size and morphology.[11–18] During a typical PISA process, a stabilizer block is chain-extended by polymerizing a soluble monomer to produce amphiphilic BCPs, which *in situ* self-assemble into nano-objects with diverse morphologies. Recently, developing novel PISA strategies for constructing nanowires has attracted great research interest.[19–22] For example, Guan *et al.* reported scalable production of nanowires *via* polymerization-induced

hierarchical self-assembly of stilbene-containing BCPs.[23] Boott *et al.* reported the formation of cylindrical micelles at high solids (up to 25%) *via* polymerization-induced crystallization-driven self-assembly.[24] Despite great progress in preparation of BCP nanowires, synthesis of BCP helical nanowires *via* PISA has been rarely reported.

Recently, fluoropolymers have been extensively employed in PISA due to their unique properties, such as high lipophobicity, high chemical stability, low surface energy, and low refractive index.[25,26] In an overwhelming majority of PISA formulations, fluorinated polymers are adopted as the core-forming blocks because of their outstanding solvophobicity. In particular, semi-fluorinated poly(meth)acrylates bearing side groups with high numbers of fluorocarbons exhibit excellent liquid crystalline nature and have been exploited in ordered self-assembly.[27,28] For example, Huo and co-workers reported that cylindrical micelles could be readily prepared by dispersion of semi-fluorinated-containing monomer in a wide range of block compositions.[29] Shen *et al.* reported on facile preparation of ellipsoidal morphologies through dispersion polymerization of heptade-cafluorodecyl methacrylate.[30] Despite these significant developments, using fluorinated polymers as the stabilizer blocks in PISA has been relatively undeveloped because of their poor solubility.

Jinnai and co-workers have demonstrated that a marginally solubilized block within a triblock copolymer can induce nanoparticle fusion, finally resulting in a morphology transition from spheres into helices.[31] Considering the marginal solubility of short fluoropolymer in ethanol, we envision that inserting small amounts of fluorinated units within a stabilizer block can significantly improve the interaction between nanoparticles. Thus, the hierarchical self-assembly of BCP nanoparticles might be induced,[32] producing helical nanowires. Herein, in

[a]State Key Laboratory of Ophthalmology, Optometry and Vision Science, School of Ophthalmology and Optometry, School of Biomedical Engineering, Wenzhou Medical University, Wenzhou 325027, PR China

[b]Engineering Research Center of Clinical Functional Materials and Diagnosis & Treatment Devices of Zhejiang Province, Wenzhou Institute, University of Chinese Academy of Sciences, Xinsan Road, Longwan District, Wenzhou 325001, PR China. E-mail: shenjl@wiucas.ac.cn

Paper

this work, we aim to testify our hypothesis *via* PISA using a fluorinated stabilizer block. As demonstrated in Scheme 1A, a copolymer comprising of 2-(dimethylamino)ethyl methacrylate (DMAEMA) and 2,2,2-trifluoroethyl methacrylate (TFEMA) units was used to mediate the reversible addition–fragmentation chain transfer (RAFT) dispersion polymerizations of 2-(perfluorohexyl)ethyl methacrylate (FHEMA) in ethanol. The morphology of the resulting nano-objects was systematically investigated by dynamic light scattering (DLS), scan electron microscopy (SEM), and transmission electron microscopy (TEM).

Results and discussion

The fluorinated stabilizer block was firstly synthesized by RAFT homogeneous copolymerization of DMAEMA and TFEMA. The targeting degree of polymerization (DP) of DMAEMA and TFEMA was 45 and 5, respectively. The total monomer conversion was determined to be 60% by ^{1}H NMR spectroscopy. After precipitation in petroleum ether and vacuum drying, pure polymer powder was obtained. The chemical structure of purified polymer powder was characterized by ^{1}H NMR spectroscopy, which is shown in Fig. 1A. By comparing the integral ratio of signal e ($\delta = 4.09$ ppm) and d ($\delta = 4.37$ ppm), the actual repeated units of DMAEMA and TFEMA were determined to be 27 and 3, respectively. Gel permeation chromatography (GPC) analysis in Fig. 1B shows a narrow molecular weight distribution ($M_w/M_n = 1.19$) and good agreement between theoretical and experimental molecular weights ($M_{n,NMR} = 5028$ g mol^{-1}, $M_{n,GPC} = 5201$ g mol^{-1}). The TFEMA/DMAEMA ratio was deemed important because too much TFEMA units would lead to aggregation of the stabilizer blocks before dispersion polymerization. Therefore, the P(DMAEMA$_{27}$-*co*-TFEMA$_3$)-CTA
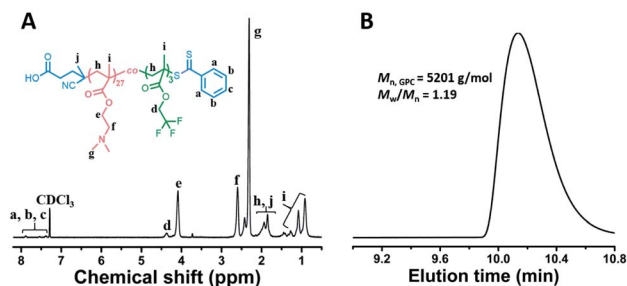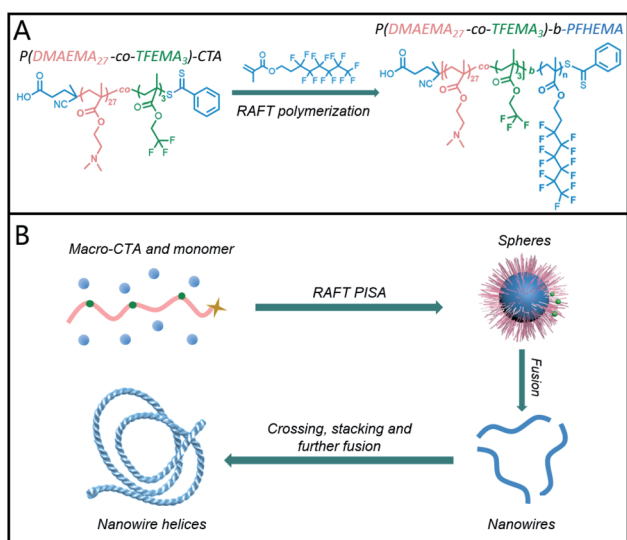

Fig. 1 (A) ^{1}H NMR spectrum of P(DMAEMA$_{27}$-*co*-TFEMA$_3$)-CTA in CDCl$_3$; (B) GPC trace of P(DMAEMA$_{27}$-*co*-TFEMA$_3$)-CTA.

ethanol solution was characterized by DLS to determine if the polymer was adequately dissolved in ethanol. DLS result in Fig. S1† indicated that no aggregates formed. As the inset image shown, the polymer solution is clear and transparent, indicating that no colloidal dispersion formed.

Then, the dispersion polymerizations of FHEMA mediated by P(DMAEMA$_{27}$-*co*-TFEMA$_3$)-CTA were conducted at 20% solid content in ethanol. The polymerization conditions and results were summarized in Table 1. Near quantitative FHEMA conversions after 16 h were confirmed by ^{1}H NMR spectroscopy. After precipitation and subsequent vacuum drying, pure P(DMAEMA$_{27}$-*co*-TFEMA$_3$)-*b*-PFHEMA$_n$ BCPs were obtained. Their BCP compositions were characterized by ^{1}H NMR spectroscopy using a mixed solvent CDCl$_3$/CF$_2$ClCFCl$_2$ (3 : 2, v/v), which allowed efficient dissociation of PFHEMA block aggregation. As shown in Fig. 2, the signal e′ ($\delta = 4.37$ ppm) increased with the increasing of targeting PFHEMA DP, indicating successful RAFT dispersion polymerizations.

The morphology of the resulting P(DMAEMA$_{27}$-*co*-TFEMA$_3$)-*b*-PFHEMA$_n$ nano-objects was initially characterized by SEM. As shown in Fig. 3A, when the DP of PFHEMA was 20, helical nanowires with several micro-meters in length were observed. The handedness of the helical nanowires was confirmed based on SEM image. We observed that the handedness kept

Scheme 1 (A) Schematic demonstration of RAFT dispersion polymerization of FHEMA using P(DMAEMA$_{27}$-*co*-TFEMA$_3$) as the stabilizer block and (B) formation of helical nanowires *via* hierarchical self-assembly.

Table 1 Summary of the dispersion polymerizations of FHEMA in ethanol mediated by P(DMAEMA$_{27}$-*co*-TFEMA$_3$)-CTA at 70 °C

Feed ratio[a]	Solid (%)	Conv.[b] (%)	$D_{h,app}$[c]/nm	PDI[c]
1/20/0.3	20	99	28–383	0.20–0.76
1/30/0.3	20	99	40–408	0.17–0.72
1/40/0.3	20	99	71–316	0.21–0.63
1/50/0.3	20	99	98–448	0.14–0.86
1/60/0.3	20	99	124–350	0.17–0.59

[a] Molar ratio (P(DMAEMA$_{27}$-*co*-TFEMA$_3$)-CTA/FHEMA/AIBN). [b] Monomer conversions determined by ^{1}H NMR spectroscopy in CDCl$_3$. The corresponding peaks of HDFDMA completely disappeared in the ^{1}H NMR spectra, indicating near quantitative monomer conversions (99%). [c] The average value of apparent hydrodynamic diameter ($D_{h,app}$) and the polydispersity index (PDI) of the nano-objects confirmed by DLS characterizations with the block copolymer concentration of 0.1% (1 mg mL^{-1}). The left column: determined immediately after PISA synthesis; the right column: determined after aging for 7 days.
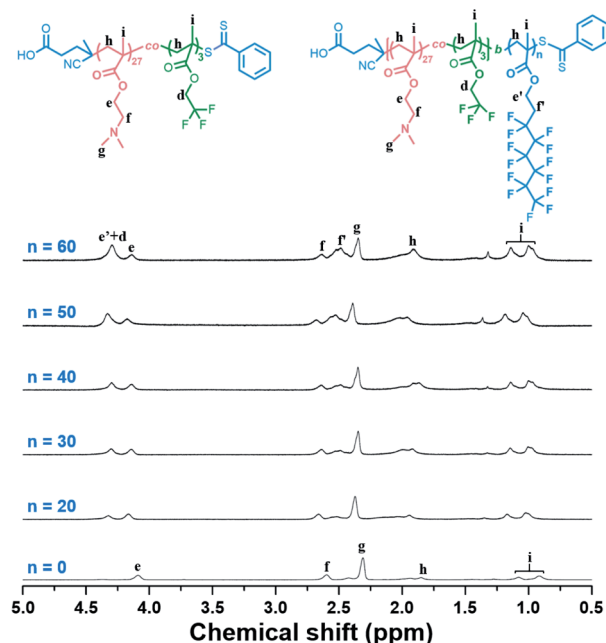
Fig. 2 ^{1}H NMR spectra of P(DMAEMA$_{27}$-co-TFEMA$_3$)-b-PFHEMA$_n$ in CDCl$_3$/CF$_2$ClCFCl$_2$ (3 : 2, v/v). n = 0, 20, 30, 40, 50, and 60, respectively.

dichroism analysis in Fig. S2,† no Cotton effect was observed for the helical nanowire ethanol solution. This is probably because the helical nanowires were resulted from the twist of the single nanowire without preferred twisting sense. After all, the BCPs synthesized in PISA exhibited no chirality and no chiral molecules were added in PISA synthesis as well. In addition, it can be observed that helical nanowires can fold into nest-like structures (Fig. 3B). Interestingly, spheres together with curved nanowires were observed in Fig. 3C, suggesting that the spheres seemed to undergo a fusion into helical nanowires. In addition to SEM characterizations, TEM analysis in Fig. 3D also indicated that the length of the helical nanowires extended to as long as several micro-meters. It can be clearly observed in Fig. 3E and F that the helical nanowires were multiple-strand helices, which consist of the twist of thinner nanowires. Note that the number of single nanowires in a helix varied between different helices. For example, the helix in Fig. 3E seems to consist of four thinner nanowires while the one in Fig. 3F has much more thinner nanowires. Therefore, the width and pitch of helix varied widely among the different helices in the same sample.

As the SEM image in Fig. 4A shown, helical nanowires can be still obtained when the DP of PFHEMA slightly increased to 30. TEM image in Fig. 4B also indicated the formation of micron-

Fig. 3 SEM (A–C) and TEM (D–F) micrographs of P(DMAEMA$_{27}$-co-TFEMA$_3$)-b-PFHEMA$_{20}$ helical nanowires.

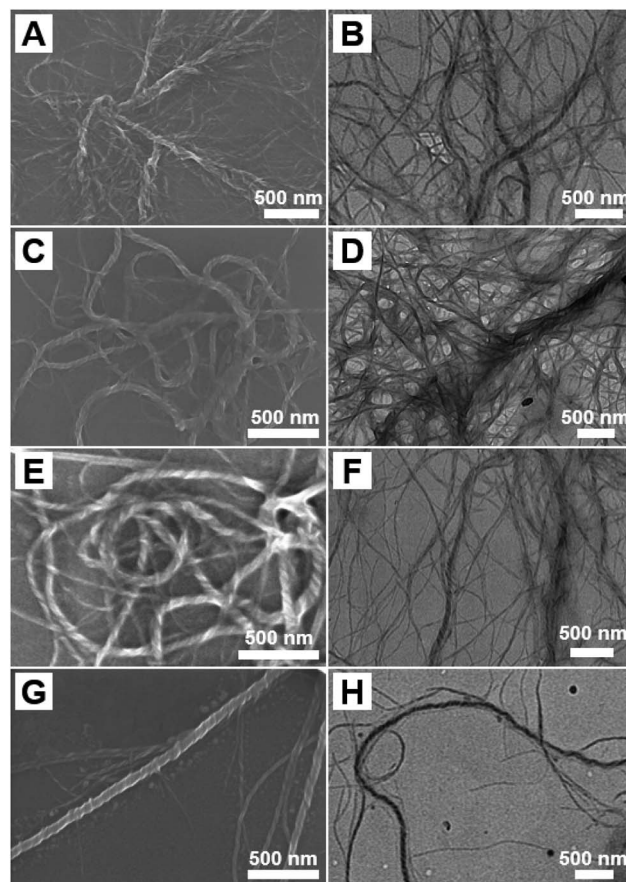**Fig. 4** SEM and TEM micrographs of P(DMAEMA$_{27}$-co-TFEMA$_3$)-b-PFHEMA$_n$ helical nanowires: (A and B) n = 30; (C and D) n = 40; (E and F) n = 50; (G and H) n = 60.

unchanged within an individual helix. The inset image in Fig. 3A indicated that there were both left- and right-handed ones in the same SEM sample. As demonstrated by circular

long helical nanowires. Interestingly, helical nanowires can be readily produced as the DP of PFHEMA finally increased to 60, which were shown in Fig. 4C–H. To the best of our knowledge, this is the first time that helical nanowires can be synthesized by PISA. Usually, the polymeric helical nanostructures were produced *via* self-assembly of chiral BCPs or induced by chiral molecules. Thus, the molecular chirality can be amplified by self-assembly, resulting helical nanostructures with supramolecular chirality. For instance, Lu *et al.* successfully fabricated double helices with controlled handedness *via* the self-assembly of an achiral BCP induced by ᴅ- and ʟ-tartaric acid.[33] Considering that no chiral factor was introduced in our PISA formulation, it can be rationally concluded that the helical nanostructure was not caused by chirality amplification. We speculated that the TFEMA unit within the stabilizer block led to the formation of helical nanowires. Dupont *et al.* reported successful preparation of double and triple helices through the self-assembly of an achiral ABC triblock copolymer.[31] In their self-assembly system, the selected solvents are good for C block, poor for B block, and marginal for A block. A fusion mechanism for helices was proposed. Spheres formed initially and then fused into cylinders after aging for several days. During aging, the different cylinders underwent crossing, stacking and further fusion into helices. They described that the marginally solubilized block A functioned as glue between different cylinders to attract one another.

We carefully examined our experimental details. We found that both TEM and SEM analysis indicating helical nanowires were conducted seven days after PISA synthesis while the DLS analysis was performed immediately after PISA synthesis. As shown in Table 1, the P(DMAEMA$_{27}$-*co*-TFEMA$_3$)-*b*-PFHEMA$_n$ nano-objects exhibit an average apparent hydrodynamic diameter ($D_{h,app}$) from 28 to 124 nm with narrow distribution (polydispersity index (PDI) below 0.21). However, both $D_{h,app}$ and PDI significantly increased after aging for several days. These DLS results seemed to indicate that spheres formed initially and then underwent a morphology transition into helical nanowires. In order to testify our hypothesis, PISA synthesis of P(DMAEMA$_{27}$-*co*-TFEMA$_3$)-*b*-PFHEMA$_n$ (n = 20 and 30, 20% solids in ethanol at 70 °C) was strictly repeated. DLS and TEM samples were prepared and analyzed immediately after PISA synthesis. As shown in Fig. 5, both DLS results and TEM images revealed that only spherical nanoparticles formed and no helical nanostructures were observed. As a control experiment, a dispersion polymerization of FHEMA with DP 30 was carried out using a PDMAEMA$_{31}$ stabilizer block, of which the ^{1}H NMR spectrum and GPC trace were shown in Fig. S3.† TEM analysis in Fig. S4† indiacted that spheres remained after aging for 7 days, which further confirmed that TFEMA units are key factors for the formation of helical nanowires. In fact, dispersion polymerizations of FHEMA mediated by a PDMAEMA stabilizer have been systematically investigated by Huo *et al.* and helical nanostructures were not observed.[29]

Very similar to the work of Dupont *et al.*,[31] ethanol as the solvent in our PISA synthesis is good for PDMAEMA units, poor for PFHEMA block, and marginal for TFEMA units. Therefore, similar mechanism for the formation of helical nanowires can
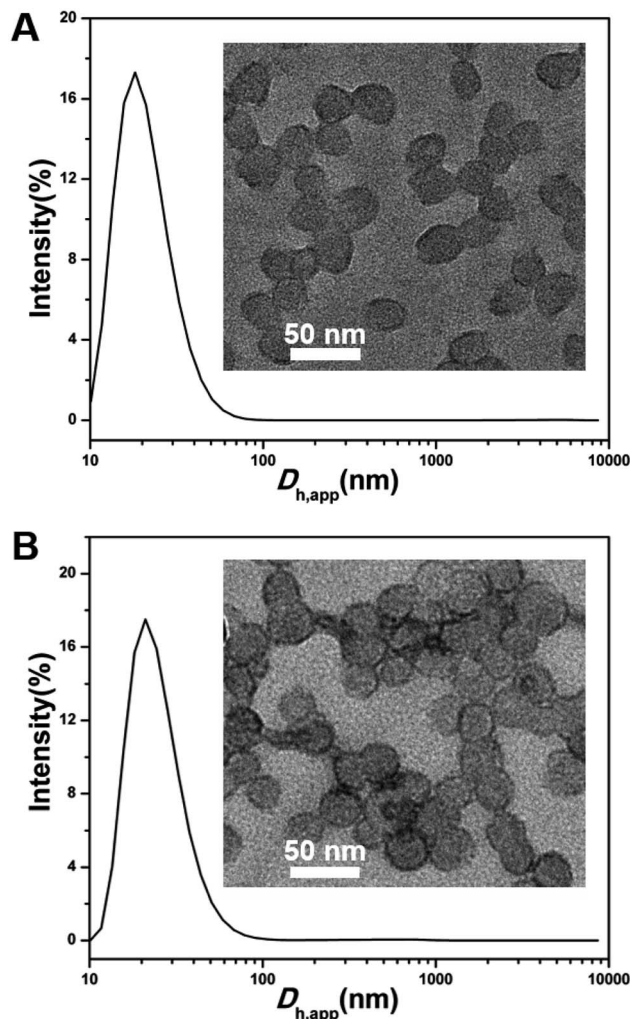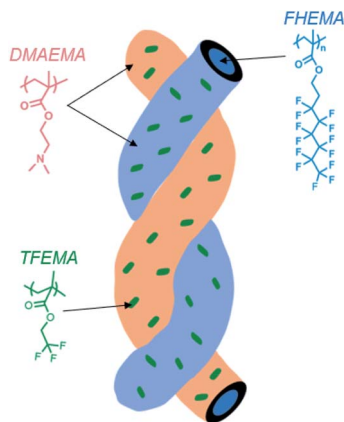

Fig. 5 DLS results of P(DMAEMA$_{27}$-*co*-TFEMA$_3$)-*b*-PFHEMA$_n$ BCP nano-objects determined immediately after PISA synthesis: (A) n = 20; (B) n = 30. The as-synthesized nano-objects dispersions *via* PISA were diluted to 0.1% (1 mg mL^{-1}) by ethanol for DLS characterization.

be proposed. Firstly, with the growth of the PFHEMA block, the resulting P(DMAEMA$_{27}$-*co*-TFEMA$_3$)-*b*-PFHEMA$_n$ BCPs initially *in situ* self-assembled into spheres during PISA synthesis. After aging for seven days, the as-synthesized spheres preferred to fuse into nanowires. Moreover, during aging, the different single nanowire underwent crossing, stacking and further fusion into helices induced by the marginally solubilized TFEMA units. To some extent, the TFEMA units randomly distributed within the stabilizer block functioned as glue between different nanowires to attract one another, which was depicted in Scheme 2. Thus, the nanowires aggregated and twisted into multiple helices so that the contact between TFEMA units and ethanol can be reduced.

To demonstrate the generality of our strategy for synthesizing helical nanowires, another two kinds of monomers were utilized in dispersion polymerizations mediated by P(DMAEMA$_{27}$-*co*-TFEMA$_3$) stabilizer block. The monomers were heptadecafluorodecyl methacrylate (HDFDMA) and lauryl

Scheme 2 Schematic demonstration of the chain packing during the formation of nanowire helices.

methacrylate (LMA), respectively (Scheme S1†). Recently, HDFDMA, a semi-fluorinated methacrylate monomer bearing bulking and rigid side group is broadly adopted in the synthesis of one-dimensional nanostructures through PISA due to their excellent liquid crystalline nature. However, helical nanowires were never reported so far when using a homopolymer as the stabilizer block.[29] In our work, a dispersion polymerization of HDFDMA using P(DMAEMA$_{27}$-co-TFEMA$_3$) as the stabilizer was conducted in ethanol at 20% solid content. As we expected, ellipsoidal nanoparticles formed initially and then underwent a morphology transition to helical nanowires after aging for seven days, which is shown in Fig. 6A and B. The size of ellipsoidal nanoparticles was statistically analyzed, which is shown in Fig. S5.† The formation of ellipsoidal nanoparticles can be attributed to the intrinsic ordering of PHDFDMA blocks.[30,34–38]

Fig. 6 SEM micrograph and DLS result of P(DMAEMA$_{27}$-co-TFEMA$_3$)-b-PHDFDMA$_{30}$ (A and B) and P(DMAEMA$_{27}$-co-TFEMA$_3$)-b-PLMA$_{30}$ (C and D) nano-objects synthesized at 20% solids content. Note: SEM samples were characterized after aging for seven days while DLS and TEM samples were characterized immediately after PISA synthesis. TEM samples were stained by phosphotungstic acid (PTA).

Similarly, a dispersion polymerization of LMA mediated by P(DMAEMA$_{27}$-co-TFEMA$_3$)-CTA was carried out in ethanol at 20% solid content. As shown in Fig. 6C and D, P(DMAEMA$_{27}$-co-TFEMA$_3$)-b-PLMA$_{30}$ BCP nano-objects also exhibited a morphology evolution from spheres to helical nanowires during aging.

In summary, a new strategy for constructing helical nanowires was developed via dispersion polymerizations mediated by a fluorinated random copolymer stabilizer. Ultralong nanowires with helical structures can be readily produced in a wide range of block compositions. In addition, the generality of our strategy was well testified by expanding monomer types. It can be clearly observed that the helical nanowires were mostly multiple-strand helices, which consist of the twist of thinner nanowires. A fusion mechanism was proposed. Spheres initially formed during PISA and then underwent a fusion into helical nanowires after aging for days. We speculate that the marginally dissolved TFEMA units within the stabilizer block functioned as glue between different nanowires. Thus, the nanowires aggregated and twisted into multiple helices so as to reduce the contact between TFEMA units and ethanol. To the best of our knowledge, it is the first time to report helical nanowires in PISA. It should be noted that no chiral agent was introduced in our work. We believe this work will provide a general strategy for constructing nanowire helices through PISA of achiral BCPs.

Experimental

Materials

2,2′-Azobis(2-methylpropionitrile) (AIBN, 99%) was purchased from Sigma-Aldrich. Heptadecafluorodecyl methacrylate (HDFDMA, 98%), 2-(perfluorohexyl)ethyl methacrylate (FHEMA), 2-(dimethylamino)ethyl methacrylate (DMAEMA, 99%), 2,2,2-trifluoroethyl methacrylate (TFEMA, 98%) and lauryl methacrylate (LMA, 98%) were purchased from Shanghai Aladdin Bio-Chem Technology. CDCl$_3$ (99.8%) and CF$_2$ClCFCl$_2$ (99.5%) were purchased from Shanghai Macklin Biochemical. All the monomers were passed through an Al$_2$O$_3$ column to remove the inhibitor prior to polymerizations. The chain transfer agent 4-cyanopentanoic acid dithiobenzoate (CPADB, 97%) was purchased from Shanghai Macklin Biochemical.

Characterization

Monomer conversions and chemical structure of the purified polymers were analyzed by ^{1}H NMR spectroscopy on a Bruker AV 400 MHz spectrometer. The core of the nanowire comprised of FHEMA blocks was hydrophobic, lipophobic and highly compact. Therefore, CF$_2$ClCFCl$_2$ was utilized as a cosolvent together with CDCl$_3$ to sufficiently dissolve fluoro-containing block copolymer nanoparticles. GPC measurements were performed on a Waters Alliance e2695 GPC system equipped with a Styragel guard column (WAT054415, 30 × 4.6 mm), two Org separation columns consisting of D2500 (300 × 8 mm) and D5000 (300 × 8 mm). Detection was made with a 2414 refractive index detector (Waters Alliance), a Viscotek 302/305 UV detector (Malvern Instruments), and a Viscotek TDA 305-020 LALS/RALS
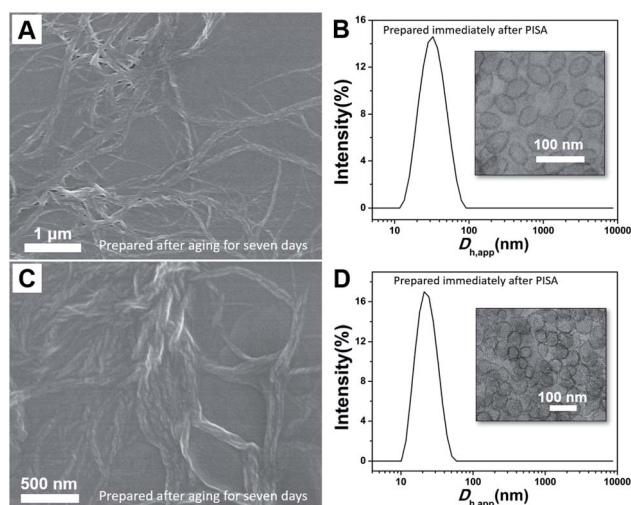
detector (Malvern Instruments). Tetrahydrofuran (THF, HPLC grade) was used as the eluent at a flow rate of 1 mL min^{-1}. To prepare GPC samples, 6–10 mg pure polymer powder was dissolved in 1 mL THF and filtered through a 0.20 μm Millipore filter. The apparent hydrodynamic diameter of the nano-objects was characterized by DLS analysis on a Malvern ZS90 with a He–Ne laser (633 nm, 4 mW) at a 90° angle. The as-synthesized nano-objects dispersions via PISA were diluted to 0.1% (1 mg mL^{-1}) in a disposable cuvette using ethanol and analyzed immediately. The viscosity was 1.748 cP and the refractive index was 1.366. The temperature for all DLS characterizations was 25 °C and the equilibration time was 120 seconds. Autocorrelation functions were analyzed by the cumulants method to calculate the Z-average hydrodynamic diameter and polydispersity index (PDI). Circular dichroism analysis was conducted on a Chirascan Plus. The morphology of the nano-objects was characterized by TEM on a Jeol 200CX microscope (200 kV) and SEM on a SU8010 microscope. The polymer concentration for all the TEM and SEM samples is 0.2 mg mL^{-1}. To prepare TEM samples stained by PTA, the nanoparticle-loaded grids were first dried for 15 minutes, followed by deposition of a small drop of PTA aqueous solution (0.5%). After 20 minutes, excess of PTA was washed away by water, and the TEM samples were dried overnight at 40 °C.

Synthesis of macromolecular chain transfer agent P(DMAEMA$_{27}$-co-TFEMA$_3$)

CPADB (0.213 g, 0.762 mmol), DMAEMA (5.4 g, 34.28 mmol), TFEMA (0.642 g, 3.82 mmol), and AIBN (25.1 mg, 0.152 mmol) were added into a glass vial and subsequently dissolved in 7.3 mL 1,4-dioxane. After the solution was bubbled with nitrogen for 30 minutes in an ice bath, the glass vial was placed into an oil bath at 70 °C and stirred at 500 rpm. After 5 h of polymerization under nitrogen, the glass vial was removed from the oil bath and the resulting solution was exposed to air to terminate the polymerization. The total monomer conversion was determined to be 60% by ^{1}H NMR spectroscopy. The pure polymer powder was obtained by precipitation in petroleum ether for three times and vacuum drying. The ratio of TFEMA units to DMAEMA units was determined by comparing the integral ratio of signal d ($\delta = 4.09$ ppm) and e ($\delta = 4.37$ ppm).

Synthesis of macromolecular chain transfer agent PDMAEMA$_{31}$

CPADB (0.213 g, 0.762 mmol), DMAEMA (6.0 g, 38.1 mmol), and AIBN (25.2 mg, 0.152 mmol) were added into a glass vial and subsequently dissolved in 7.25 mL 1,4-dioxane. After the solution was degassed with nitrogen for 30 minutes in an ice bath, the glass vial was placed into an oil bath at 70 °C and stirred at 500 rpm. After 5 h of polymerization under nitrogen atmosphere, the resulting solution was exposed to air to terminate the polymerization. The conversion of DMAEMA was determined to be 62% by ^{1}H NMR spectroscopy. The pure polymer powder was obtained by precipitation in petroleum ether for three times and vacuum drying.

Dispersion polymerizations mediated by P(DMAEMA$_{27}$-co-TFEMA$_3$)-CTA

The ethanolic synthesis of P(DMAEMA$_{27}$-co-TFEMA$_3$)-PFHEMA$_{20}$ helical nanowires at 20% solid content was described as a representative example. In brief, P(DMAEMA$_{27}$-co-TFEMA$_3$)-CTA (0.08 g, 15.9 μmol), FHEMA (0.137 g, 318 μmol), and AIBN (0.52 mg, 3.2 μmol) were added to a glass vial and dissolved in 1.05 mL ethanol. In addition, 20 μL of DMF as inner standard agent was added into the polymerization mixture. Before polymerization, 20 μL of polymerization mixture was withdraw as the sample of 0 h for ^{1}H NMR spectroscopy in CDCl$_3$. After the solution was bubbled with N$_2$ in an ice bath 5 minutes, the glass vial was placed into an oil bath at 70 °C with a stirring speed of 500 rpm. After 16 h of polymerization under nitrogen, the glass vial was removed from the oil bath and the solution was exposed to air to quench the radical. The resulting polymerization mixture was characterized again by ^{1}H NMR spectroscopy, which was denoted as the sample of 16 h. FHEMA conversions can be calculated by comparing the integral ratio of DMF and FHEMA before and after polymerization. The corresponding peaks of FHEMA completely disappeared in the ^{1}H NMR spectrum, indicating near quantitative monomer conversions. Purified P(DMAEMA$_{27}$-co-TFEMA$_3$)-b-PFHEMA$_n$ block copolymer was obtained by precipitation in petroleum ether and drying under vacuum. The BCPs compositions were characterized by ^{1}H NMR spectroscopy in a mixture of CDCl$_3$/CF$_2$ClCFCl$_2$ (3 : 2, v/v).

Author contributions

Qiumeng Chen, Yahui Li, and Ming Liu performed the experiments. Xuan Wu, Jianliang Shen and Liangliang Shen designed the project and performed the data analysis. Liangliang Shen wrote the paper. All authors discussed the results.

Conflicts of interest

There are no conflicts to declare.

Acknowledgements

References

1 M. Liu, L. Zhang and T. Wang, Chem. Rev., 2015, 115, 7304–7397.
2 Y. Wang, J. He, X. Mu, D. Wang, B. Zhang, Y. Shen, M. Lin, C. Kübel, Y. Huang and H. Chen, ACS Nano, 2017, 11, 5538–5546.

3 E. Yashima, N. Ousaka, D. Taura, K. Shimomura, T. Ikai and K. Maeda, *Chem. Rev.*, 2016, **116**, 13752–13990.

4 J. D. Watson and G. S. Stent, *The Double Helix: A Personal Account of the Discovery of the Structure of DNA*, Atheneum, New York, 1980.

5 B. Brodsky and J. A. M. Ramshaw, *Matrix Biol.*, 1997, **15**, 545–554.

6 A. Klug, *Philos. Trans. R. Soc., B*, 1999, **354**, 531–535.

7 T. Wen, H.-F. Wang, M.-C. Li and R.-M. Ho, *Acc. Chem. Res.*, 2017, **50**, 1011–1021.

8 R.-M. Ho, Y.-W. Chiang, S.-C. Lin and C.-K. Chen, *Prog. Polym. Sci.*, 2011, **36**, 376–453.

9 R.-M. Ho, M.-C. Li, S.-C. Lin, H.-F. Wang, Y.-D. Lee, H. Hasegawa and E. L. Thomas, *J. Am. Chem. Soc.*, 2012, **134**, 10974–10986.

10 P. Xu, L. Gao, C. Cai, J. Lin, L. Wang and X. Tian, *Angew. Chem., Int. Ed.*, 2020, **59**, 14281–14285.

11 M. J. Derry, L. A. Fielding and S. P. Armes, *Prog. Polym. Sci.*, 2016, **52**, 1–18.

12 X. Wang, L. Shen and Z. An, *Prog. Polym. Sci.*, 2018, **83**, 1–27.

13 F. D'Agosto, J. Rieger and M. Lansalot, *Angew. Chem., Int. Ed.*, 2020, **59**, 8368–8392.

14 H. Sun, W. Cao, N. Zang, T. Clemons, G. Scheutz, Z. Hu, M. Thompson, Y. Liang, M. Vratsanos, X. Zhou, W. Choi, B. Sumerlin, S. Stupp and N. C. Gianneschi, *Angew. Chem., Int. Ed.*, 2020, **59**, 19136–19142.

15 L. P. D. Ratcliffe, M. J. Derry, A. Ianiro, R. Tuinier and S. P. Armes, *Angew. Chem., Int. Ed.*, 2019, **58**, 18964–18970.

16 F. Lv, Z. An and P. Wu, *Nat. Commun.*, 2019, **10**, 1–7.

17 T. Lückerath, K. Koynov, S. Loescher, C. J. Whitfield, L. Nuhn, A. Walther, C. Barner-Kowollik, D. Y. W. Ng and T. Weil, *Angew. Chem., Int. Ed.*, 2020, **59**, 15474–15479.

18 X. Cheng, T. Miao, L. Yin, Y. Ji, Y. Li, Z. Zhang, W. Zhang and X. Zhu, *Angew. Chem., Int. Ed.*, 2020, **59**, 9669–9677.

19 S. Guan and A. Chen, *ACS Macro Lett.*, 2020, **9**, 14–19.

20 X. Zhang, S. Boisse, C. Bui, P.-A. Albouy, A. Brulet, M.-H. Li, J. Rieger and B. Charleux, *Soft Matter*, 2012, **8**, 1130–1141.

21 X. S. Wang, G. Guerin, H. Wang, Y. S. Wang, I. Manners and M. A. Winnik, *Science*, 2007, **317**, 644–647.

22 A. M. Oliver, J. Gwyther, C. E. Boott, S. Davis, S. Pearce and I. Manners, *J. Am. Chem. Soc.*, 2018, **140**, 18104–18114.

23 S. Guan, W. Wen, Z. Yang and A. Chen, *Macromolecules*, 2020, **53**, 465–472.

24 C. E. Boott, J. Gwyther, R. L. Harniman, D. W. Hayward and I. Manners, *Nat. Chem.*, 2017, **9**, 785–792.

25 A. Vitale, R. Bongiovanni and B. Ameduri, *Chem. Rev.*, 2015, **115**, 8835–8866.

26 T. Soulestin, V. Ladmiral, F. D. Dos Santos and B. Améduri, *Prog. Polym. Sci.*, 2017, **72**, 16–60.

27 X. Li, B. Jin, Y. Gao, D. W. Hayward, M. A. Winnik, Y. Luo and I. Manners, *Angew. Chem., Int. Ed.*, 2016, **55**, 11392–11396.

28 X. Li, Y. Gao, X. Xing and G. Liu, *Macromolecules*, 2013, **46**, 7436–7442.

29 M. Huo, D. Li, G. Song, J. Zhang, D. Wu, Y. Wei and J. Yuan, *Macromol. Rapid Commun.*, 2018, **39**, 1700840.

30 L. Shen, H. Guo, J. Zheng, X. Wang, Y. Yang and Z. An, *ACS Macro Lett.*, 2018, **7**, 287–292.

31 J. Dupont, G. Liu, K. Niihara, R. Kimoto and H. Jinnai, *Angew. Chem., Int. Ed.*, 2009, **48**, 6144–6147.

32 Y. Lu, J. Lin, L. Wang, L. Zhang and C. Cai, *Chem. Rev.*, 2020, **9**, 4111–4140.

33 X. Lu, J. Li, D. Zhu, M. Xu, W. Li and Q. Lu, *Angew. Chem., Int. Ed.*, 2018, **57**, 15148–15152.

34 M. Huo, G. Song, J. Zhang, Y. Wei and J. Yuan, *ACS Macro Lett.*, 2018, **7**, 956–961.

35 S. Guan, C. Zhang, W. Wen, T. Qu, X. Zheng, Y. Zhao and A. Chen, *ACS Macro Lett.*, 2018, **7**, 358–363.

36 Y. Li, Q. Lu, Q. Chen, X. Wu, J. Shen and L. Shen, *RSC Adv.*, 2021, **11**, 1729–1735.

37 A. P. Soto, J. B. Gilroy, M. A. Winnik and I. Manners, *Angew. Chem., Int. Ed.*, 2010, **49**, 8220–8223.

38 Z. M. Hudson, C. E. Boott, M. E. Robinson, P. A. Rupar, M. A. Winnik and I. Manners, *Nat. Chem.*, 2014, **6**, 893–898.